CHAPTER 6

TIME HORIZON-BASED MODEL PREDICTIVE VVO IN PRESENCE OF ELECTRIC VEHICLE CHARGING LOADS

6.1 Introduction

The rapid increase in the installation of DERs and higher integration of flexible loads [electric vehicles (EVs)] in distribution grid are the major opportunities and challenges for utility operators. The existing electric power infrastructure is not yet ready to adopt the large change in topologies and such integrations. Although enabling CVR in the presence of PV provides significant savings, the system performance is profoundly affected by uncertainties and intermittency associated with PV power generation and load demand. Previous efforts [30], [138] have included the impact of uncertainty in their VVO formulation; however, they have not analyzed its impact on the CVR savings. Moreover, their methodology enables control action only in a centralized manner. A centralized manner works well for a fixed time horizon interval, but it might be inflexible for fast-response events such as PV intermittency. Hence, a multi-time horizon Volt/VAR regulation has introduced in [84], [139]. However, these studies do not analyzed the CVR impact under flexible EV loads.

In the present scenario, EV penetration is one of the fastest growing advanced components of modern distribution systems worldwide. Therefore, DNOs and distribution network planners have the challenge to determine the new control algorithms that coordinate with other components of a network for efficient and optimal operation. In this context, a recent study [140] has presented the agent-based approach for EV charging load modelling, including the aggregated behavior of vehicles and human nature. Besides, the impact of

PHEVs charging on the distribution system and electrified transportation system has also been explored in [141]. Investigations for optimal EV charging scheduling with distributed renewable power and distributed energy management system for Vehicle-to-Grid (V2G) operation has been carried out in [142], [143]. Apart from the use of smart inverter in the solar PV system, the EV charging stations inverter can also play a key role to act as a mobile storage to feed and consume the active and reactive power from and to the distribution grid. In [144]-[146] the various centralized and local control strategies for reactive power compensation through EV charging station in low and medium voltage distribution system has been studied. Though, the authors of [145], [146] have included the impact of EVs on their VVO methodology. However, very few have [147] examined the impact of EVs in the presence of CVR. Though, in [145], [146], authors have analyzed the impact of EV loads penetration while obtaining the optimal VVC devices set points through smart grid VVO engine assessing the optimal V2G impact on power losses and switching cost. However, this study does not include effect of DER and CVR in their VVO formulation in presence of EV loads. Moreover, the method also focused on only centralized control in slow time scale operation.

In this chapter, a multi-time horizon-based model predictive VVO (MP-VVO) engine along with autonomous Volt/VAR droop (VVD) controls has been introduced in the real-time framework. The main objective of proposed VVO is to minimize the CVR cost, network losses cost, and VVO devices operating cost. In addition, provision of VAR support from V2G has also been assessed under centralized VVO operation and voltage control in the local domain due to sudden change in DER power output. The proposed MP-VVO methodology is beneficial for optimal CVR execution, scheduling the VVC devices [both

traditional and power electronics (PE) based], and maintaining the feeder voltage profile even in the presence of EV charging loads. Moreover, the autonomous VVD controller is very useful to handle the smart inverter's (both PV and EV) VAR dispatch under the cloud transients on PV-based DER power output to control the local voltage during the real-time operation. In addition, the proposed control algorithms also tolerate the uncertainties and forecast error present in network loads and DER outputs.

6.2 Time Horizon based Control

Electric power system operation and control are executed in different time horizons and different time scales. In distribution grid, there are mainly two categories of VVO devices, which are traditional and PE-based devices. OLTC, AVR and CBs are traditional VVO that are controlled in slow time scale (from hour to minutes). The PE-based voltage regulation devices, such as smart inverters that can be controlled in slow as well as fast time scale (within few seconds) both. The switched traditional controllers are rescheduled only a few times in a day due to limited cycles operation constraints and the slow variation in load demand. Therefore, control action of these devices in slow time scale is enough for VVC execution. However, during a sudden change in network behaviour and DERs, power output fluctuation may generate the detrimental impact on grid operation. Hence, there is a need of fast-acting distributed control devices, such as smart inverter, that can respond quickly during the fast time scale operation to avoid the undesirable issues. Therefore, in this chapter, a time horizon-based model predictive control methodology has been introduced that can work under both slow and fast time scales. To do so, the entire time horizon (T) is divided into prediction time horizon (Tp) slots. The prediction time horizon (Tp) is further sectionalized into q subslots having control time horizon (Tc) with a sampling time step (dt) as shown in

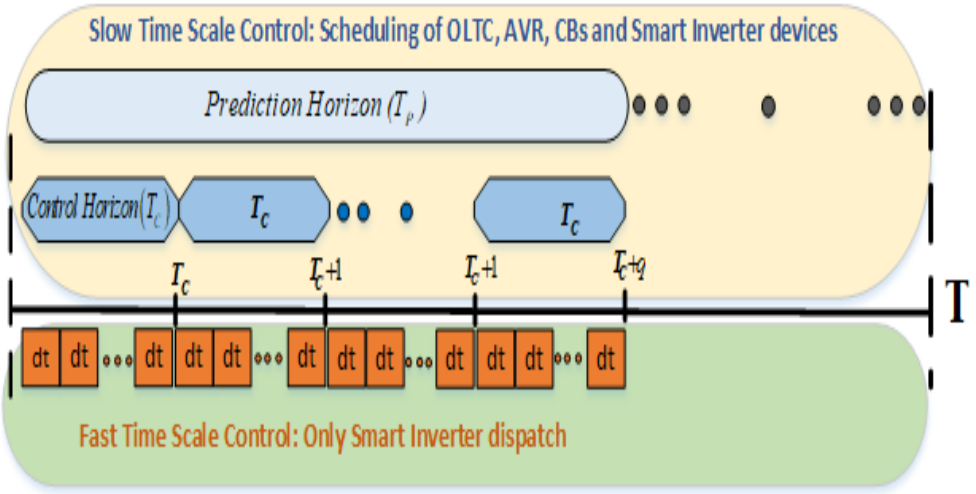

Figure 6.1 Time horizon-based model predictive control

Figure 6.1. For instance, the value of T is 24 h followed by each *Tp* of 1 h. If the value of *q* is four then *Tc* would be 15-min interval with dt time step. A detailed discussion on both timescales is given as follows.

6.2.1 *STSC: Centralized Approach*

In STSC, the aggregated control algorithms have been applied to coordinate and dispatch the control set points over a finite period at the substation level. Therefore, this control is alternatively referred to as a centralized control scheme. In STSC, VVO devices can be scheduled in different prediction and control horizons (Tp and Tc), having time intervals minutes to hour. In present study, Tp of 1 h and Tc of 15-min interval have been taken to reschedule the set points/dispatches of OLTC/AVR, CBs, and smart inverters in optimal manner under STSC operation, as shown in Figure 6.1.

6.2.2 FTSC: Local Control

In STSC, the VVO devices are scheduled for a defined time horizon. During this time span. (set in STSC), however, the deviation in PV power output with respect to the forecasted value can be observed because of unexpected situations, such as transient cloud movements or a solar eclipse. Consequently, it might cause a violation of voltage limits. Therefore, fast control action is needed to maintain the voltage profile limits during the reduction of PV power output. The smart inverters have the ability to respond quickly [89] and they can absorb and inject reactive power. An autonomous approach is used to control the inverter dispatch in a real-time framework. In this study, the dt simulation time step (within the Tc range) is considered to control the only smart inverter dispatch in fast time scale, as shown in Figure 6.1.

6.3 Model Predictive VVO

Generally, the model predictive approach is used to handle the defined finite horizon control problem in optimal manner over the prediction horizon (*Tp*), as shown in Figure 6.2.

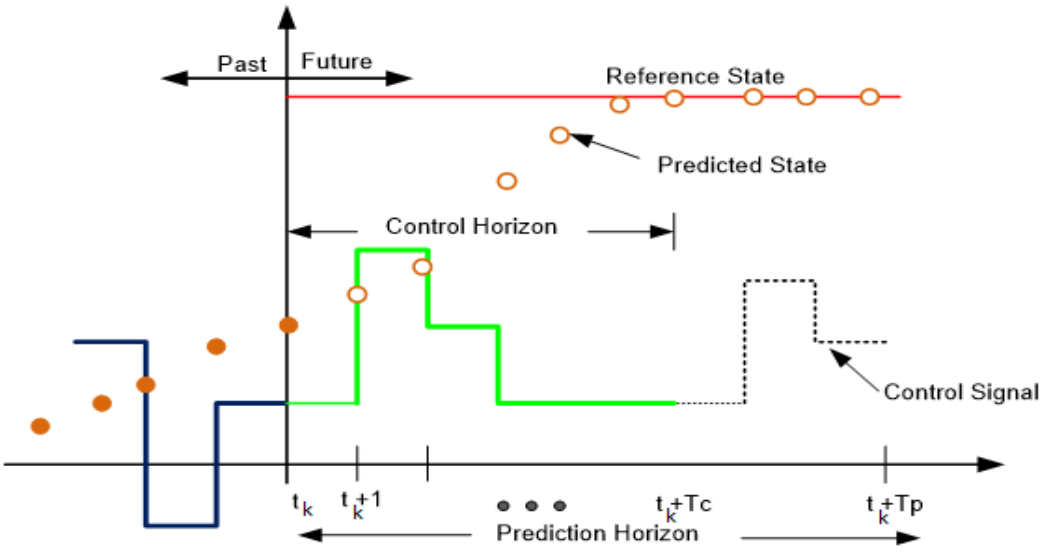

Figure 6.2. Illustration of model predictive control

The achieved control set points are sent to the system to execute the control action over the control horizon Tc ($Tc \leq Tp$). In order to obtain the sequence of control sets, the optimal control problem has been solved based on forecasted data considering the uncertainty and forecasting error. The control variables that lie within the range of $tk + T_c$ (control region) have been implemented for the execution of the system operation and the rest have been discarded. The above-mentioned procedure is repeated using updated observations at $t_k + 1$. Details of uncertainty modeling of loads and DER have been described as under.

6.3.1 Load Prediction Uncertainty

The probability density function is commonly used for representing the load forecast uncertainty of the forecasted load. The information available in literature reveals that normal distribution is an effective method to generate uncertainty in forecasted load consumptions [138]. The forecasted load is defined as the mean value of the normal distribution, and 2% of the expected load is set as the standard deviation.

6.3.2 PV Irradiance Uncertainty Prediction

Solar irradiance is a vital and determinant parameter on which the solar power generated from the PV module depends. Therefore, the highest amount of uncertainty in PV power generation is exhibited by irradiance itself. In order to model the irradiance uncertainty, the beta distribution is considered in this study [138]. The mean of the beta distribution has been defined as Id_{norm}, which represents the value of current irradiance prediction in a time horizon. The standard deviation is a function of the mean value. The variable mean, and standard deviation depend on *A* and *B* parameters. For a predicted irradiance (Id_{norm}), *A* and *B* are the parameters used for defining beta function as follows:

$$F_{Idnorm_{j,t}}(I) = I^{(A-1)}(1-I)^{(B-1)} \tag{6.1}$$

The above-mentioned beta function models the occurrence of irradiance values I when a certain prediction value Id_{norm} has been forecasted. The connection of *A* and *B* with mean and variance for each time instant of the prediction interval have been expressed as follows:

$$Mean(\mu) = \frac{Id_{norm_{j,t}}}{Id_{base}} = \frac{A_{j,t}}{A_{j,t} + B_{j,t}} \tag{6.2}$$

$$Variance(\sigma^2) = \frac{A_{j,t}B_{j,t}}{(\mathrm{A}_{j,t} + B_{j,t})^2(\mathrm{A}_{j,t} + B_{j,t} + 1)} \tag{6.3}$$

The value of *A* and *B* and can be determined using equations (6.2) and (6.3) with the uncertainty produced by equation (6.1).

6.4 EV loads and Charging Stations

The impact of EVs at various consumption levels and different places, such as workplaces, houses, and shopping malls has directed a significant change in daily demand of the network [11]. With the emergence of the smart inverter, EV charging stations have a powerful feature to provide the reactive power support to the grid. Enabling of EVs with this feature leads to the increase in network capacity, reduction in system losses, and enhancing the voltage profile [145], [146]. But these benefits are subjected to system constraints, such as load rise, uncertainty in loads, and DER power generations. In order to achieve the above-mentioned benefits from EV, the role of EV inverter is very crucial. The EV charging stations equipped with smart inverters have the ability to work in different operating modes [146] (shown in Figure 6.3), given as follows.

- *Mode 1*: On the border between Quadrants I and IV (P > 0, Q = 0)
- *Mode 2:* Quadrants I (P > 0, Q > 0)
- *Mode 3*: On the border between Quadrants I and II (P = 0, Q > 0)

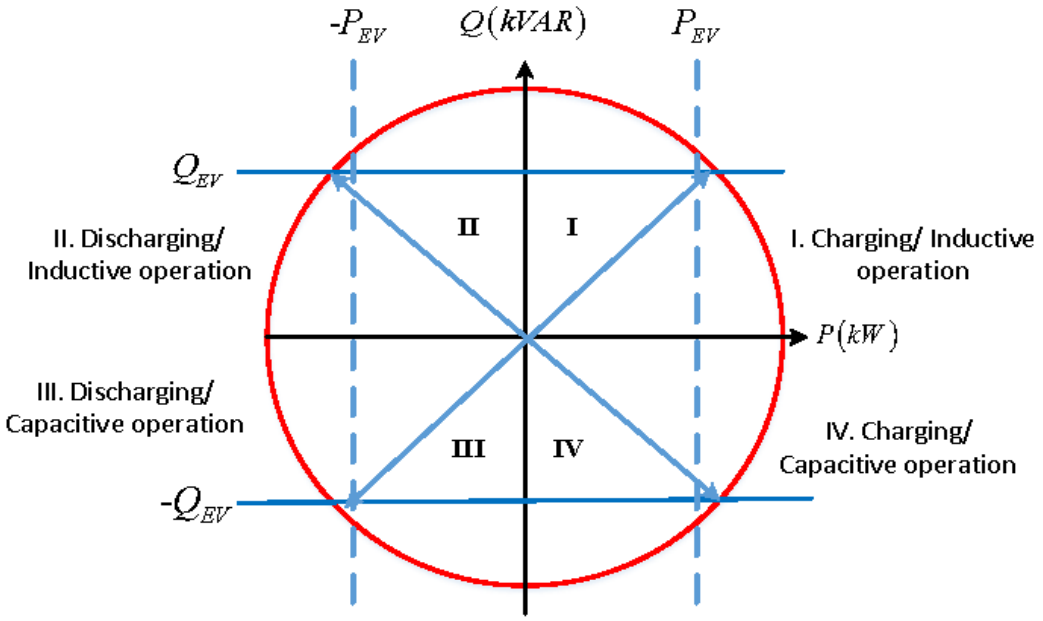

Figure 6.3 Active and reactive power capability of EV inverter

- *Mode 4*: Quadrants II (P < 0, Q > 0)
- *Mode 5*: On the border between Quadrants II and III (P < 0, Q = 0).
- *Mode 6:* Quadrants III (P < 0, Q < 0).
- *Mode 7:* On the border between Quadrants III and IV (P =0, Q < 0). 238
- *Mode 8*: Quadrants IV (P > 0, Q < 0).

Generally, EV operates in P > 0, Q = 0 *Mode 1* (i.e., unity power factor), which exhibits that EV consumes only the real power from the grid. Another possible operating *Mode 8* for EV charging station inverter is to inject the VAR into the grid, while consuming real power for EV battery charging. Apart from the above-mentioned operating Mode 7, there is an operation scenario in which charging station can inject the reactive power to the grid when there is no EV connected to the charging station. Thus, in near future, charging station may be a possible candidate for reactive power support.

6.5 Problem Formulation: Stochastic Optimization

In the present scenario, energy efficiency and demand reduction are the major concerns of DNO. In order to achieve this, an advanced way of CVR operation has been incorporated into VVO models, where multiple voltages regulating devices, such as OLTC, CBs, and smart inverter of PV/EV are coordinated optimally without violating the system constraints. In the slow timescale, enabling CVR and total operating cost are the main objectives. In the fast timescale, the goal is to control the voltage locally.

6.5.1 Optimization Model

In this optimization model, the MP- VVO tries to minimize the CVR cost, network losses cost, and VVO devices operating cost, simultaneously. The proposed MP-VVO objective function can be formulated, as shown in the following:

$$f = \min \sum_{t=t_k}^{t_k+T_P} \left[C_{CVR}^t + C_{loss}^t + C_{VR}^t + C_{OLTC}^t + C_{CB}^t + C_{SI,Qpv}^{t,} + C_{SI,Q_{EV}}^t \right] \quad (6.4)$$

Where,

$$C_{CVR}^t = \alpha \sum_{i \in \Omega_{bus}} C_{cvr,t} \times \frac{1}{\Delta E_{i,t}} \quad 6.5)$$

$$C_{loss}^t = \beta \sum_{br \in \Omega_{br}} C_{loss,t} \times P_{br,loss}^t \quad (6.6)$$

$$C_{VR}^t = \gamma \sum_{vr \in \Omega_{vr}} C_{vr,t} \times X_{vr}^t \quad (6.7)$$

$$C_{OLTC}^t = \gamma \sum_{l \in \Omega_{oltc}} C_{l,t} \times X_{l,oltc}^t \quad (6.8)$$

$$C_{CB}^{t} = \gamma \sum_{cb \in \Omega_{CB}} C_{cb,t} \times Q_{i,cb}^{t} \tag{6.9}$$

$$C_{SI,Qpv}^{t} = \pi \sum_{i \in \Omega_{pv}} C_{grid,t} \times Q_{i,pv}^{t,inv} \tag{6.10}$$

$$C_{SI,QEV}^{t} = \pi \sum_{i \in \Omega_{EV}} C_{grid,t} \times Q_{i,EV}^{t,inv} \tag{6.11}$$

In equation (6.4), $C_{CVR}^{t}, C_{loss}^{t}, C_{VR}^{t}, C_{OLTC}^{t}$, and C_{CB}^{t} represents the CVR cost, power losses cost, operating cost of voltage regulator, OLTC, and CBs respectively. $C_{SI,Qpv}^{t}$ and $C_{SI,QEV}^{t}$ represents smart inverter reactive compensation cost of PV and EV respectively. Similarly, symbols of Ω_{bus}, Ω_{br}, Ω_{vr}, Ω_{oltc}, Ω_{CB}, Ω_{pv} and Ω_{EV} represents the set of all buses, branches, branches with VRs, OLTCs, buses with CB, PV and EV respectively. α, β, γ and π are the weighting factors and their summation should be equal to 1.

6.5.2 Control Variables

The following control variables are considered in the optimization problem.

- Tap position of OLTC/AVR (T_P^t)
- CBs reactive power ($Q_{i,cb}^{t}$).
- PV reactive power dispatch ($Q_{i,pv}^{t,inv}$).
- EV charging station reactive power dispatch ($Q_{i,EV}^{t,inv}$)

The output of the present optimization is the control set points of OLTC/AVR, CBs, and smart inverter in such a way that to achieve the aforementioned goal, the problem has been formulated in slow and FTSC objectives.

6.5.3 System Constraints

Equation (6.4) is subjected to the following system operating constraints

- *Transformer/regulator tap constraints:* The tap range of OLTC transformers/AVR and tap position are given in (6.12) and (6.13) respectively.

$$0.90\,\text{p.u.} \le \text{Tap} \le 1.1\,\text{p.u.} \tag{6.12}$$

$$\text{Tap} = \left\{1 \pm \left(\frac{\Delta V_{tr}}{100}\right) \times T_P^t\right\} \tag{6.13}$$

where $T_P^t \in \{-16,....0.....16\}$, ΔV_{tr} is 0.625 increments in voltage at each step and T_P^t is tap position.

- *Voltage constraints:* Minimum and maximum voltage (*Vmin*, *Vmax*) at *i*th node should remain within limits as expressed in the following:

$$V_{\min} \le V_i^t \le V_{\max},\ V_i^t \in [0.95 - 1.05]\,\text{p.u.} \tag{6.14}$$

- *Capacitor bank constraints:* Reactive power supplied by *i*th CB ($Q_{i,cb}^t$) is determined using equation (6.15)

$$Q_{i,cb}^t = Sw_{i,cb}^t \times \Delta Q_{i,cb}^t ;\ \forall i \in \Omega_{CB} \tag{6.15}$$

where, $Sw_{i,cb}^t = \{0,1,2,3.....,Sw_{i,cb}^{\max}\}$, $Sw_{i,cb}^t$ $\Delta Q_{i,cb}^t$ and $Sw_{i,cb}^{\max}$ are the switching step number, variation in reactive power per step and available maximum number of switching steps at *i*th CB, respectively.

- *PV smart inverter constraints:* The reactive power supplied by *i*th PV inverter ($Q_{i,pv}^{t,inv,stsc}$) during slow time scale period (t) is determined using the following

$$Q_{i,pv}^{t,inv,stsc} = N_{i,pv} \times \Delta Q_{i,\mathrm{pv}}^{t,inv};\ \forall i \in \Omega_{pv} \tag{6.16}$$

where, $N_{i,\mathrm{pv}} = \left\{0,1,2,3.....,\mathrm{N}_{i,\mathrm{pv}}^{\max}\right\}$, $N_{i,\mathrm{pv}}$, $\Delta Q_{i,\mathrm{pv}}^{t,inv}$ and $\mathrm{N}_{i,\mathrm{pv}}^{\max}$ are the switching step number, variation in reactive power per step and available maximum number of switching steps at *i*th PV system.

The available ($Q_{i,pv}^{t,inv,\max}$) is dependent upon the real power generation for a time instance t ($P_{i,pv}^{t,inv}$) which is governed by the following

$$Q_{i,pv}^{t,inv,\max} = \sqrt{\left(S_{i,pv}^{inv,\max}\right)^2 - \left(P_{i,pv}^{t,inv}\right)^2}\ \forall i \in \Omega_{pv} \tag{6.17}$$

On the basis of $P_{i,pv}^{t,inv}$ and $S_{i,pv}^{inv,\max}$, $Q_{i,pv}^{t,inv,\max}$ is recalculated at every time period (t).

- *EV constraints:* Minimum and maximum limits of voltage, active and reactive power of EV as follows

$$V_{i,\mathrm{EV}}^{\min} \le V_{i,\mathrm{EV}}^{t} \le V_{i,\mathrm{EV}}^{\max} \tag{6.18}$$

$$0 \le P_{i,\mathrm{EV}}^{t,inv} \le P_{i,\mathrm{EV}}^{t,inv,\max} \tag{6.19}$$

$$0 \le Q_{i,\mathrm{EV}}^{t,inv} \le -Q_{i,\mathrm{EV}}^{t,inv,\max} \tag{6.20}$$

The reactive power supplied by *i*th EV inverter during slow time scale period (t) is determined using the following:

$$Q_{i,\mathrm{EV}}^{t,inv,stsc} = N_{i,\mathrm{EV}} \times \Delta Q_{i,\mathrm{EV}}^{t,inv};\ \forall i \in \Omega_{\mathrm{EV}} \tag{6.21}$$

where, $N_{i,\mathrm{EV}} = \left\{0,1,2,3.....,\mathrm{N}_{i,\mathrm{EV}}^{\max}\right\}$, $N_{i,\mathrm{EV}}$, $\Delta Q_{i,\mathrm{EV}}^{t,inv}$ and $\mathrm{N}_{i,\mathrm{EV}}^{\max}$ are the switching step

number, variation in reactive power per step and available maximum number of switching steps at *i*th EV system.

The available ($Q_{i,\mathrm{EV}}^{t,inv,\max}$) is dependent upon the real power charging load for a time instance t ($P_{i,\mathrm{EV}}^{t,inv}$) which is governed by the following

$$Q_{i,\mathrm{EV}}^{t,inv,\max} = \sqrt{\left(S_{i,\mathrm{EV}}^{inv,\max}\right)^2 - \left(P_{i,\mathrm{EV}}^{t,inv}\right)^2} \;\forall i \in \Omega_{\mathrm{EV}} \tag{6.22}$$

On the basis of $P_{i,\mathrm{EV}}^{t,inv}$ and $S_{i,\mathrm{EV}}^{inv,\max}$, $Q_{i,\mathrm{EV}}^{t,inv,\max}$ is recalculated at every time period (t).

6.6 Solution method and Procedure

6.6.1 Prediction Error and Scenario Generation

In this work, the PV power generation has been considered as DER. It is well known that the prediction models are always prone to errors. The beta distribution is used to represent solar irradiance prediction errors, as discussed in subsection 6.3.1. Based on uncertain prediction errors and forecasted power, the monte-carlo simulation has been utilized to generate scenarios (N) for solar irradiance and load consumptions. Various distributions and their parameter settings can be varied depending upon the information available regarding the system.

6.6.2 Scenario Reduction and Aggregation

The larger number of scenarios make improvement in the uncertainty model. However, it creates higher computation complexity and enhances computational time. Therefore, in this study, K-means clustering based scenario reduction technique is employed in order to reduce the number of scenarios (N'). While reducing the number of scenarios, a good amount of approximation of the system uncertainty should be maintained. In this method, the data is

clustered based on minimum distance from the centroid of each cluster. After generating N (N=500) scenarios, they have been reduced to N' (15) scenarios using K-means clustering [148] and getting 15 probability of occurrence of each scenario. After implementing the scenario reduction technique, the probability of the achieved scenarios is normalized as follows:

$$\rho_s^{norm} = \frac{\text{(Probability of occurance of one of reduced scenario)}}{\text{(Sum of porbability of occurance of reduced scenarios)}} \tag{6.23}$$

The number of scenarios N reduces to N' by deploying the above procedures. Hence, the problem defined in (6.4) could be rewritten as a stochastic optimization problem with reduced scenarios as given (6.24)

$$\min\left[\sum_{s=1}^{N'} \rho_s^{norm} \times f_s\right] \tag{6.24}$$

The VVO problem redefined in (6.24) is solved by discrete DPSO followed by the system constraints from equations (6.4) – (6.24). PSO is a population-based heuristic optimization technique [149]. The controlling parameters of DPSO used in this study are depicted in appendix C, Table C.1. The achieved optimal control set points from the above formulation are dispatched to the VVO devices for the current prediction horizon based on predicted DER outputs to minimize operating cost of VVO (in this study CVR) implementation. This procedure is repeated when different observations come at t_k + 1. Figure 6.4 shows the flowchart of the implementation of the proposed scheme.

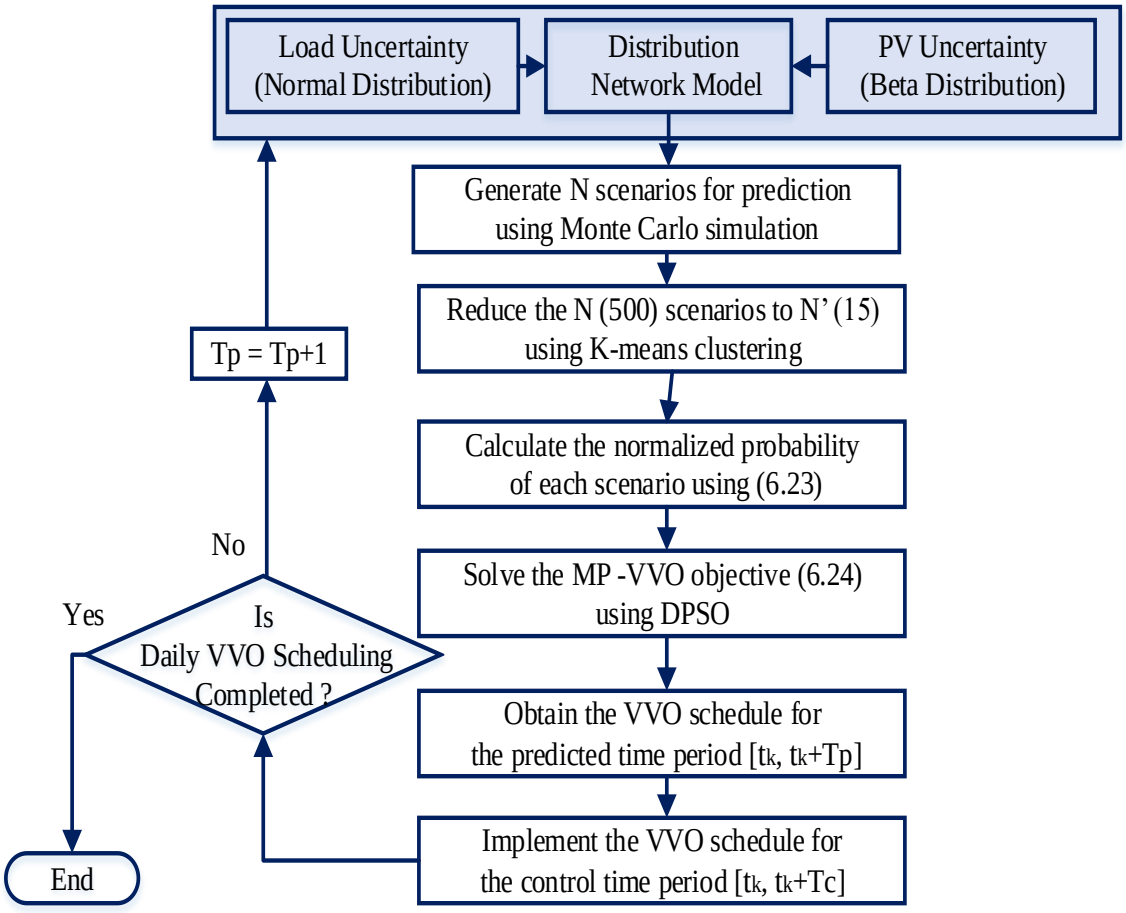

Figure 6.4 Flowchart of MP-VVO execution in STSC

6.6.3 Droop Controller for Smart Inverter

The control set points obtained from model predictive VVO can directly be implemented for CVR under STSC. However, under FTSC, the autonomous approach has been suggested. A droop-based control scheme has been deployed to enable the autonomous operation of the smart inverter to compensate the additional reactive power support. The detailed description can be seen chapter 5. The compensated reactive power ($\Delta Q_{i,PV/EV}^{t,inv,com}$) at any instant, t can be determined using equation (6.25).

$$\Delta Q_{i,\text{PV/EV}}^{t,\text{inv,com}} = \begin{cases} Q_{i,\text{PV/EV}}^{t,\text{inv,av max}} & V < V_1^{P_1} \\ \dfrac{V - V_1^{P_1}}{V_1^{P_1} - V_2^{P_2}} Q_{i,\text{PV/EV}}^{t,\text{inv,av max}} & V_1^{P_1} \le V < V_2^{P_2} \\ 0 & V_2^{P_2} \le V \le V_3^{P_3} \\ -\dfrac{V - V_3^{P_3}}{V_4^{P_4} - V_3^{P_3}} Q_{i,\text{PV/EV}}^{t,\text{inv,av max}} & V_3^{P_3} < V \le V_4^{P_4} \\ -Q_{i,\text{PV/EV}}^{t,\text{inv,av max}} & V > V_4^{P_4} \end{cases} \quad (6.25)$$

where $Q_{i,\text{PV/EV}}^{t,\text{inv,av max}}$ is the maximum available VAR capacity of smart inverter of PV/EV for droop controller at an instant t that is determined by the following:

$$Q_{i,\text{PV/EV}}^{t,\text{inv,av max}} = Q_{i,\text{PV/EV}}^{t,\text{inv,max}} - Q_{i,\text{PV/EV}}^{t,\text{inv,stsc}} \quad (6.26)$$

The total VAR support with droop controller ($Q_{i,\text{PV/EV}}^{t,\text{inv}}$) at an instant t is determined by the following

$$Q_{i,\text{PV/EV}}^{t,\text{inv}} = Q_{i,\text{PV/EV}}^{t,\text{inv,stsc}} + \Delta Q_{i,\text{PV/EV}}^{t,\text{inv,com}} \quad (6.27)$$

6.6.4 Implementation of proposed coordinated scheme

In this subsection, the coordinated operation of STSC and FTSC devices have been implemented using aggregated and autonomous approach as shown in Figure 6.5. This figure demonstrated that in centralized control, MP-VVO executes every 15 minutes interval and generate the optimal set points for STSC devices. However, in local control, droop controller runs autonomously and generates desired set points for FTSC devices in near real time operation.

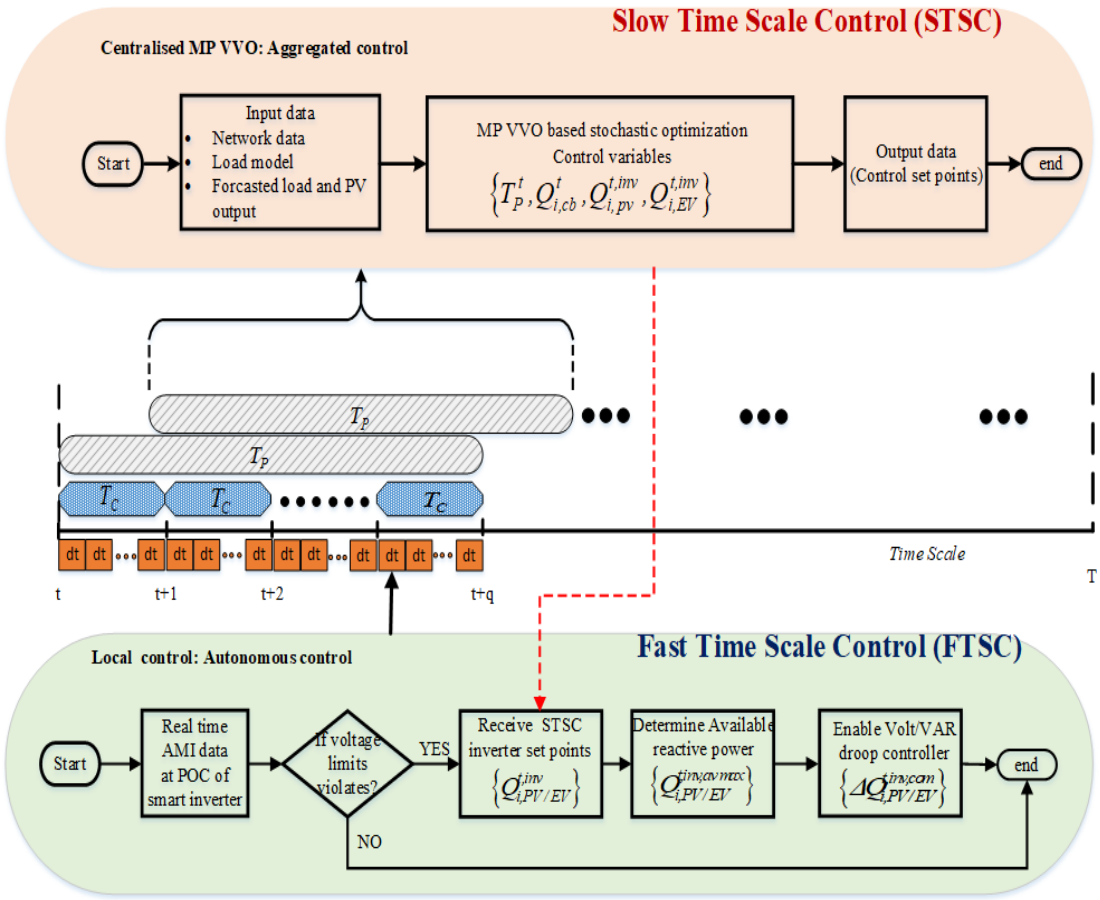

Figure 6.5 Implementation of the proposed coordinated scheme

6.7 Case Study and Simulations

6.7.1 Test system description

In order to validate the proposed VVO methodology, a modified IEEE-34 node test feeder[114] has been considered as shown in Figure 6.6. The slack bus is at the primary side of the 2.5 MVA D–Y substation transformer with 69/24.9 kV voltage rating with a fixed ratio equal to 2.56. There are two automatic voltage regulators connected between nodes 814 - 850 (AVR-1) and 852-832 (AVR-2) and each one has 16 tap increments of 0.625% at the secondary side. Two three-phase CBs are connected to buses 844 and 848 with the ratings of 300 kVAR and 450 kVAR with step variations from 0 to 3 respectively.

The additional three 3 phase PV plants at nodes 848 (PV1), 890 (PV2) and 840 (PV3) having inverter ratings 200kVA, 300kVA and 400kVA respectively. Per step reactive power variation from PV and EV charging station inverter is 10 kVAR and 5kVAR for slow time scale operation respectively. For EV charging mode, the constant power load characteristics with type 1 and type 4 [146] and charging level 2 of 6 kW power rating [142] have been assumed in this study.

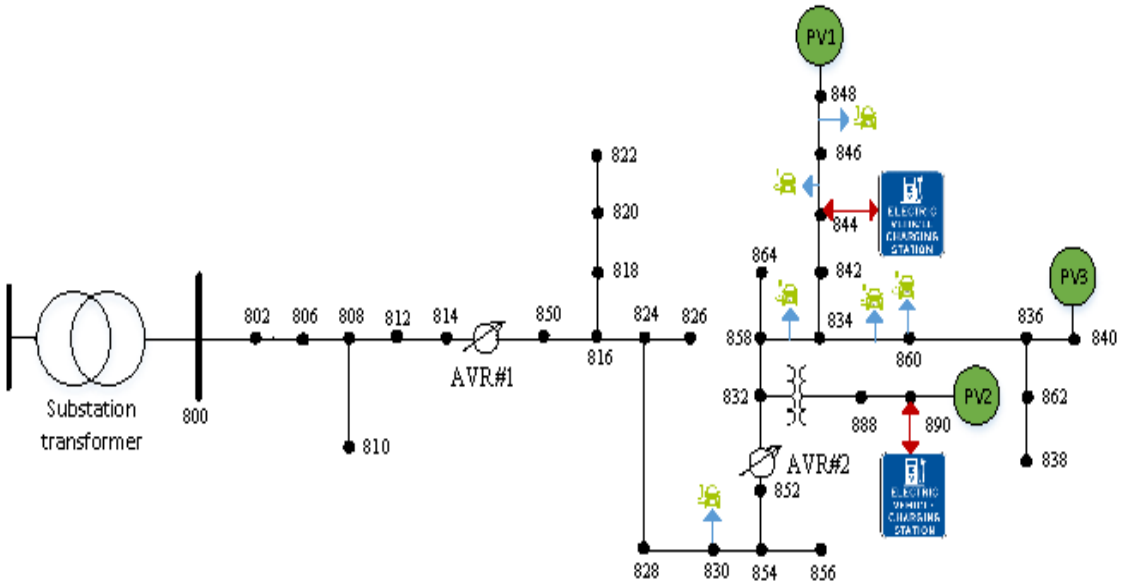

Figure 6.6 Modified IEEE 34 bus distribution system

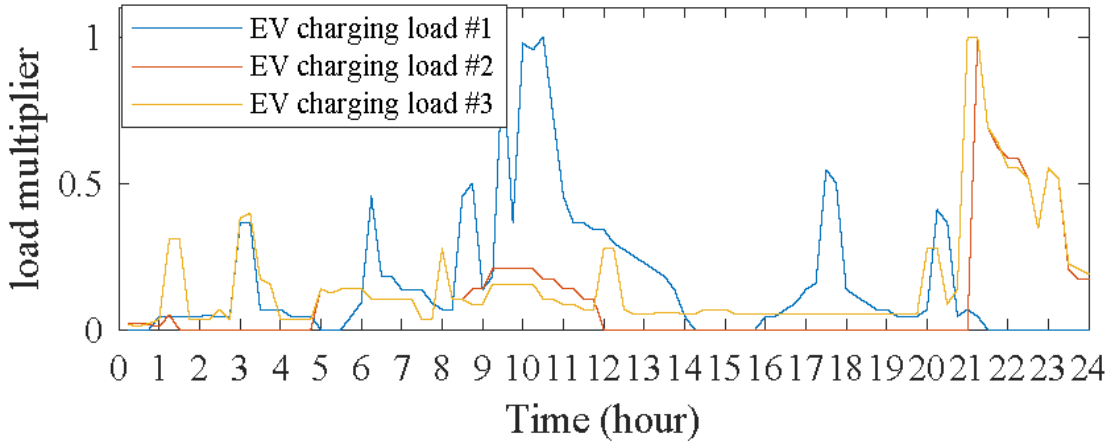

Figure 6.7 EV load profiles

Three different EV charging load profile for a typical day have been used in this study as shown in Figure 6.7. The normal EV penetration range with a maximum of 20% of the system load has been considered. For EV charging outlet and charging stations locations are referred from [141], where the authors have mapped the IEEE 34 bus system to a real-world transportation system and define the EV charging location as shown in Table 6.1. The charging points are divided into two categories. The first type charging outlet which does not participate in VAR support means they are operating in Mode1 (P>0 and Q=0) and second is charging stations that have the ability to inject and absorb the reactive power even when there is no EV is connected (i.e. Mode 7). It is further assumed that EV inverter support's reactive power only if when it has not reached its maximum allowable kW power ratings. Note that charging station 890 and 844 follows the EV charging load profile 1 and EV charging load profile 3 respectively. Rest of the EV charging outlets follow the EV charging load profile 2 as shown in Figure 6.8. The quasi-real-time load and PV profile for a typical day have been shown in Figure 6.9. Similarly, grid price has been shown in Figure 6.9. the cost parameters have been taken from [146].

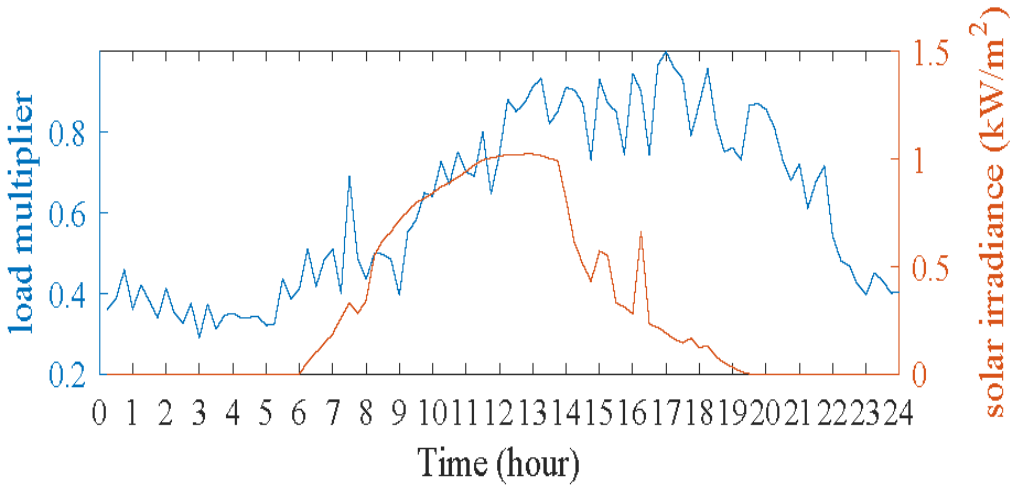

Figure 6.8 Forecasted load and solar irradiance

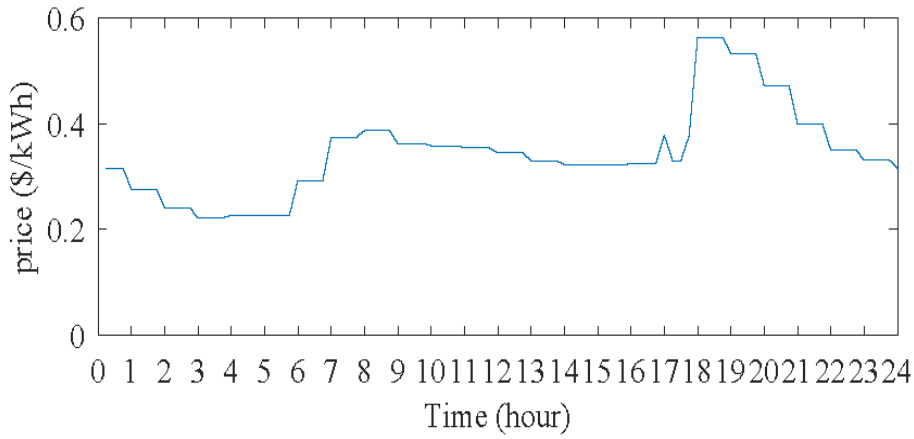

Figure 6.9 Grid price over a day

Table 6.1 EV Charging Location and Ratings

S.no.	**Location / node (a,b,c phase)**	**Maximum Rated Power**	**Charging Point (Outlet/Station)**
1	846_848b	12 kW	Outlet (Only P)
2	844_846b	6 kW	Outlet (Only P)
3	858_834b	6 kW	Outlet (Only P)
4	830c	12 kW	Outlet (Only P)
5	834_860b	6 kW	Outlet (Only P)
6	844	120 kW	Station (P, Q)
7	860	18 kW	Outlet (Only P)
8	890	180 kW	Station (P, Q)
9	834_860a	6 kW	Outlet (Only P)

6.7.2 Simulations and Results Analysis

The proposed VVO methodology has been developed in Python while the test system modeled and load flow analysis has been done in the OpenDSS platforms interfaced through the component object model (COM). The quasi-static time series simulations have been carried out for 24 hours at fifteen minutes interval for the following cases.

- Case 1: ADN without MP-VVO and without EV (Base)
- Case 2: ADN with MP-VVO
- Case 3: ADN in the presence of EV without MP-VVO
- Case 4: ADN with MP-VVO in the presence of EVs as reactive power support

- *Case 1. ADN Without MP-VVO and Without EV (Base)*

In this case the simulation has been carried out without VVO and EV penetration. The CVR has not been performed. The line drop compensation scheme has been used to execute the VVC operation. Simulation results are depicted in the second column of Table 6.2. The energy demand (E^{demand}) and energy losses (E^{losses}) of the system have been observed as 102.37 MWh, and 6.869 MWh respectively. The total operating cost of the distribution system is calculated as $29997.45 for 24 hours.

- *Case 2: ADN with MP-VVO*

In this case, proposed MP-VVO has been implemented aiming to CVR execution. Impact of EV penetrations in ADN has not been considered in this case. The results are depicted in the third column of Table 6.2. From results, it is observed that significant energy demand reduction about 5.024% and 14.383% losses reduction have, respectively, been achieved as compared to case 1. Moreover, the lowest voltage profile has also been improved, which is above the lower voltage limit (0.95 p.u.). The total operating cost of distribution network has also been reduced to $28172.327. The remarkable cost savings of about $1825.123 has been achieved after the inclusion of CVR. Reported savings in terms of energy and cost reveal the effectiveness of proposed VVO methodology for CVR execution.

- *Case 3: ADN in the Presence of EV Without MP-VVO*

This case deals with the simulation of ADN in the presence of EV penetration without involving VVO. The execution of CVR also has not been included. The load flow and VVC have been performed using a line drop compensation method. The obtained results of this case have been portrayed in the fourth column of Table 6.2. The energy demand and energy losses of the system have been observed as 107.396 and 7.625 MWh, respectively. The total operating cost of the distribution system has been calculated to be $34719.54.

Table 6.2 Results of different cases

Parameters	**Without EV**		**With EV**	
	Case 1	***Case 2***	***Case 3***	***Case 4***
E^{demand} **(MWh)**	102.37	97.226	107.396	103.821
ΔE^{demand} **(MWh)**	----	5.144	----	3.575
ΔE^{demand} **savings (%)**	----	5.024	----	3.328
E^{losses} **(MWh)**	6.869	5.881	7.625	6.587
ΔE^{losses} **(%)**	----	14.383	------	13.61
Minimum voltage (pu)	0.9252	0.9501		0.95
Cost of energy purchased from grid ($)	29348.28	27549.81	34022.83	32453.39
Active power loss cost ($)	639.77	550.01	686.16	592.91
PV SI VAR compensation cost ($)	-----	61.08	----	37.67
EV SI VAR compensation cost ($)	----	-----	----	9.404
VR, CBs switching operating cost ($)	9.4	11.2	10.55	11.8
CVR cost ($)	-----	0.227	-----	0.335
Total operating cost ($)	29997.45	28172.327	34719.54	33105.509
Cost of energy savings ($)	-----	1825.123	-----	1614.031

- *Case 4. ADN With MP-VVO in the Presence of EVs as Reactive Power Support:*

In this case, proposed MP-VVO has been utilized in the presence of EV penetration aiming to CVR execution. EV charging stations are participating partially in reactive power support. They can inject about 60% of the maximum EV KVA inverter capability. In this study, only two charging stations at nodes 890 and 844 are providing VAR support with the maximum value of 100 and 50 kVAR, respectively. The simulation results of this case have been shown in the fifth column of Table 6.2. The reported energy demand and losses of the system are 103.821 and 6.587 MWh, respectively. In comparison to Case 3, the significant reduction in energy demand and losses about 3.328% and 13.61% have, respectively, been achieved. Moreover, the total operating cost of distribution network is reduced to $33105.509, as shown in Table 6.2. The remarkable cost savings about $1614.031 have been reported after inclusion of CVR. Reported savings in terms of energy cost reveal that proposed VVO methodology works well in the presence of EV as well.

- *Minimum voltage profile under different cases*

Figure 6.10(a) shows the voltage profile of the node where the voltage is lowest without EV penetration with and without VVO impact. From this figure, it can be seen that in Case 1, the lower limit violates at different instances. Moreover, the lowest voltage varies from 1.012 to 0.9242 p.u., which is in a high range. In Case 2 operation, VVO execution with proposed method yield voltage profile improvement with less voltage deviation in the lowest voltage profile. Further, it can be clearly seen that no lower limit violation occurs with the enabling of MP-VVO during the whole operation. On the other hand, Figure 6.10(b) shows the lowest voltage profile of Cases 3 and 4, which includes the EV penetration impact. Similar to Case 1, Case 3 does not include VVO, which also results in lower voltage limit violations.

However, Case 4 operation that enabled with proposed VVO does not result in lower voltage limit violations.

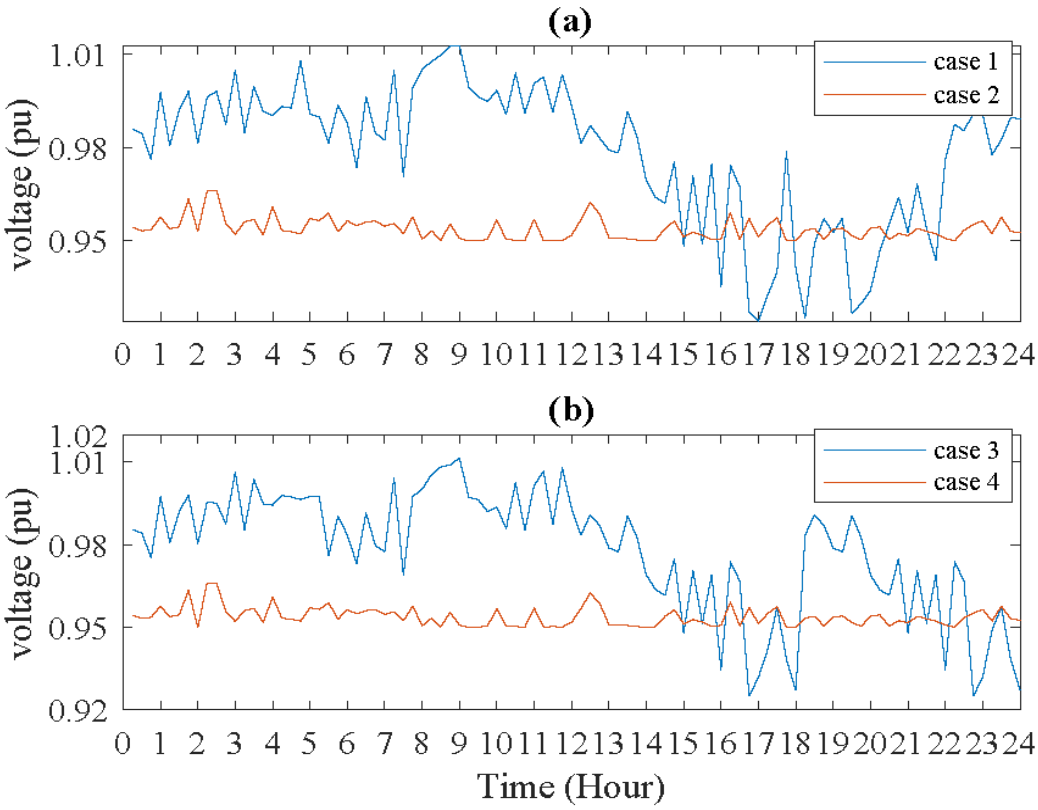

Figure 6.10: Lowest voltage under (a) *case 1* and *case 2* (b) *case 3* and *case 4*

- *Energy demand and dynamic CVR savings under different cases*

The impact of proposed VVO methodology on energy demand and CVR savings has been discussed under different cases. Figure 6.11(a) shows the varying power demand for Case 1 and Case 2, and dynamic CVR saving at each 15-min interval. Figure 6.11 shows that CVR savings are changing dynamically. It can be observed from this figure that most of the time CVR saving is reported on peak loading scenario. On the other hand, in the presence of EV in ADN, the power demand and CVR savings for Cases 3 and 4 have been shown in Figure 6.11(b). From this figure, it can be observed that the proposed VVO method reduces the

energy demand and also coordinates the EV impact in VVO to variation in load demand. At some points, the CVR saving is negative due to the constant power characteristics of EV charging loads. It is a fact that CVR has a negative impact on the constant power load characteristics. Further, in the presence of EV in ADN without VVO, i.e., Case 3, the feeder voltage suffers a higher violation of lower limit. But the execution of VVO in the presence of EV does not result in any voltage violations; it means that it increases the voltage profile of the system. As a consequence, CVR savings may or may not be positive in such conditions.

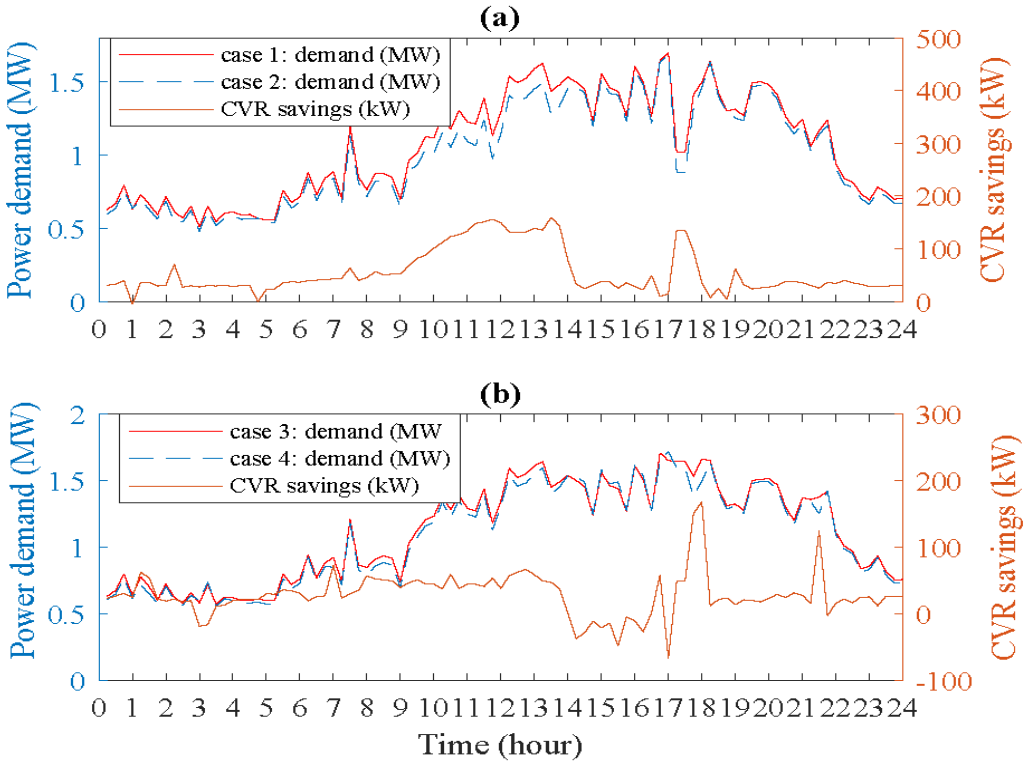

Figure 6.11. Power demand and CVR savings under (a) *case 1* and *case 2*, and (b) *case 3* and *case 4*.

- *Smart inverter reactive power support from PV and EV under different cases*

Figure 6.12 shows the optimal reactive power dispatch from PVs and EV smart inverters. These figures demonstrate that the need for reactive power is much higher in either peak

loads when there 653 is no PV power or higher penetration of EVs. The reactive power dispatch from smart inverters reduces the VAR support from capacitors. It can be said that smart inverter (PV and EV) may limit the use of CBs and emerge as a potential future candidate for VAR support in the global and local domain.

- *Illustration under FTSC: local control*

In order to validate the proposed control methodology under FTSC, the effect of cloud transient has been studied. An arbitrary instantaneous point between time intervals from 14:00 to 14:15h has been selected. The load demand is 91% of peak demand at this point and forecasted solar irradiation is 81% of the peak. During this time span, the lowest voltage profile at node 890 becomes vulnerable to any reduction in kW power. Status of VVO devices AVRs and CBs remain the same, as determined in STSC, as shown in Table 6.3. The FTSC has been applied and illustrated for two cases. The droop parameters used in this study have been shown in Appendix C in Table C.2.

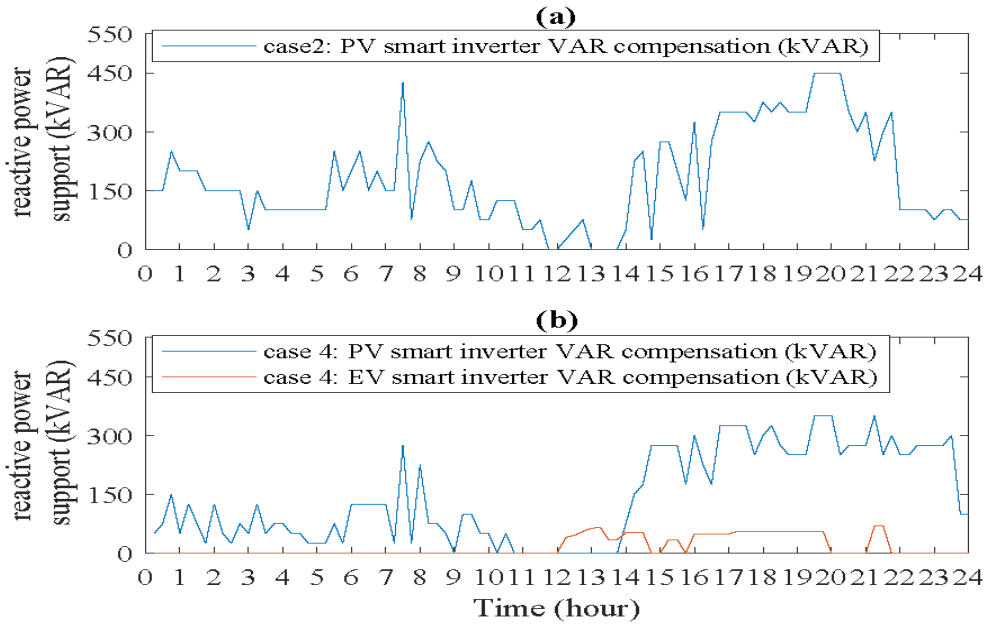

Figure 6.12. Reactive power support from PV/EV smart inverter under (a) *case 2* and (b) *case 4.*

Table 6.3: STSC set point at 14:00 h to 14:15 h

Tap position (T_P^t)	AVR-1 {1, -5, -2}; AVR-2 {5,6,6}
CBs reactive power ($Q_{i,cb}^t$).	CB_{844}{200}; CB_{848}{150}
PV reactive power dispatch ($Q_{i,pv}^{t,inv}$).	PV1 {0}; PV2{100}; PV3{0}
EV charging station reactive power dispatch ($Q_{i,EV}^{t,inv}$)	EV#1{40}; EV#2{10}

(i) *Case I. Effect of Cloud Transient in the Absence of EV:*

In this case, the sudden drop in solar irradiation from 0.81 to 0.4 kW/m^2 is observed due to the cloud movement. Accordingly, the reduction in active power from the PVs plant is reported. Hence, there is a voltage drop occurs due to such incidents. Figure 6.13 shows the drop in the lowest voltage profile with respect to fall in solar irradiation and total VAR support from PV inverters.

(ii) *Case II. Effect of Cloud Transient in the Presence of EV:*

In this case, the sudden drop in solar irradiation from 0.81 to 0.3 kW/m^2 is observed due to cloud movement in the presence of EV in ADN. Figure 6.14 shows the drop in the lowest voltage profile with respect to fall in solar irradiation. Figure 6.14 clearly demonstrates the droop control-based approach for local control that helps to mitigate the lower voltage limit violation by providing additional reactive power compensation from PV inverters up to 0.4 kW/m^2 reduction in solar irradiation. However, after further reduction, PV inverters alone are not capable of maintaining the lower voltage limit. This happens because PV inverters have already reached their maximum allowable reactive power capacity. In such conditions, EV inverters from the charging station equipped with droop control feed the additional VAR support. Figure 6.14 clearly shows that after injecting the VAR from EV inverters, the lower

voltage violations have been mitigated. It is to be noted that the limit of reactive power compensation from EV inverter should also meet their maximum allowable range. If both PV and EV inverters fail to maintain the lower feeder voltage limit, in such conditions, the operator has to reschedule the VVO set points using centralized control approach.

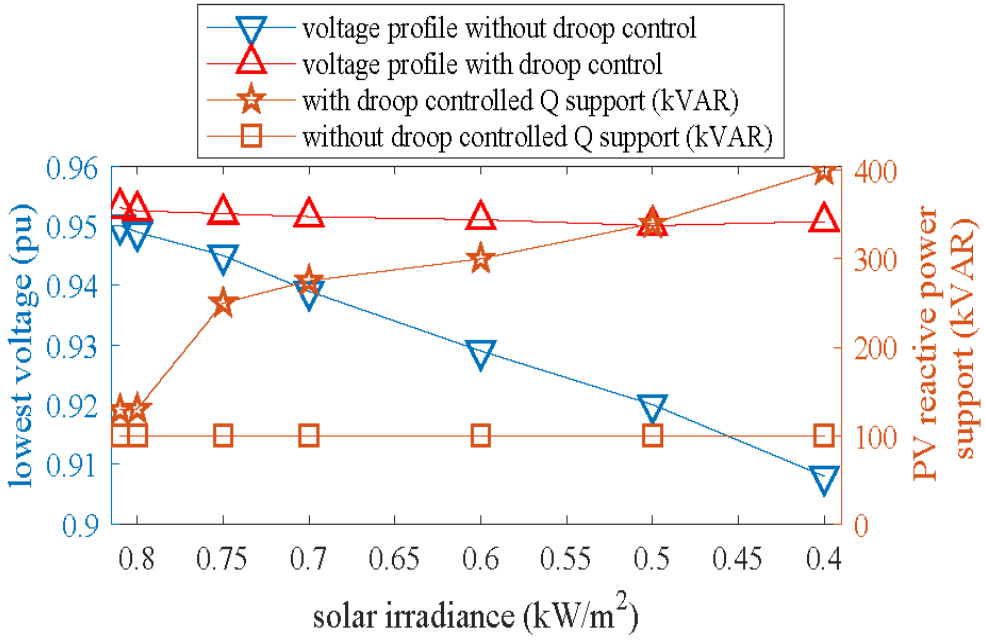

Figure 6.13 Lowest voltage profile and compensated VAR support from PV inverters

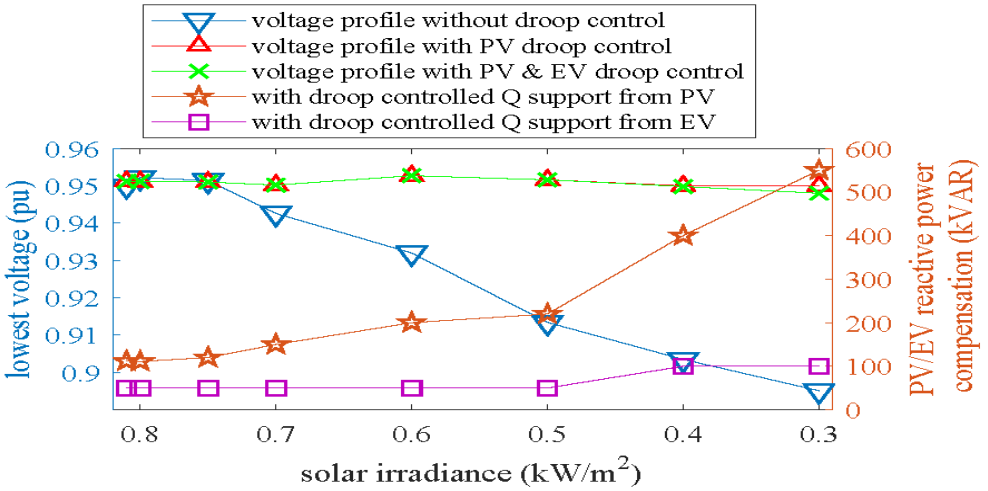

Figure 6.14. Lowest voltage profile and compensated VAR support from PV and EV inverters

6.7.3 Validation of Droop Controls in the Real-Time Simulation Platform

The droop controllers operate autonomously for local control actions in real-time. Therefore, in this study, the proposed droop control actions have been validated in a real-time simulation platform using a real-time digital simulator (RTDS).

6.7.3.1 Real-Time Simulation using RTDS

This thesis intended to use the RTDS in order to perform the real-time simulation. It has its own internal clock, unlike pure computer-based simulations. The RTDS will never stop its real-time simulations; either it does not receive the external command from other simulation platforms timely or waits for such command [150], [151]. Therefore, simulations in RTDS reflects the actual behavior of the grid operations. RTDS can be functionally divided into two main parts as software and hardware. A dedicated software named RSCAD is used to model the network and hardware is used for run time [152]. Apart from normal or Power System simulation mode (50 microsecond time step), RTDS simulator (Version 5.0 or after that) also offering a special mode of operation named as Distribution Mode with time step range of 100-200 microsecond to simulate large-scale distribution feeders in real Distribution Mode with time step range of 100-200 microsecond to simulate large-scale distribution feeders in real-time and can perform various studies and validate their controllers related to distribution system [152], [153]. Therefore, this work intends to use the *Distribution Mode* simulation to test the developed control algorithms in a large-scale test system. A schematic of RTDS Novacor, interacting with RSCAD (version 5.007)/ run time, has been shown in Figure 6.15. The simulation has been carried out in distribution mode with simulation time step (*dt*) of 120 μs. The modeling of DERs and EV loads are built using average models [153].

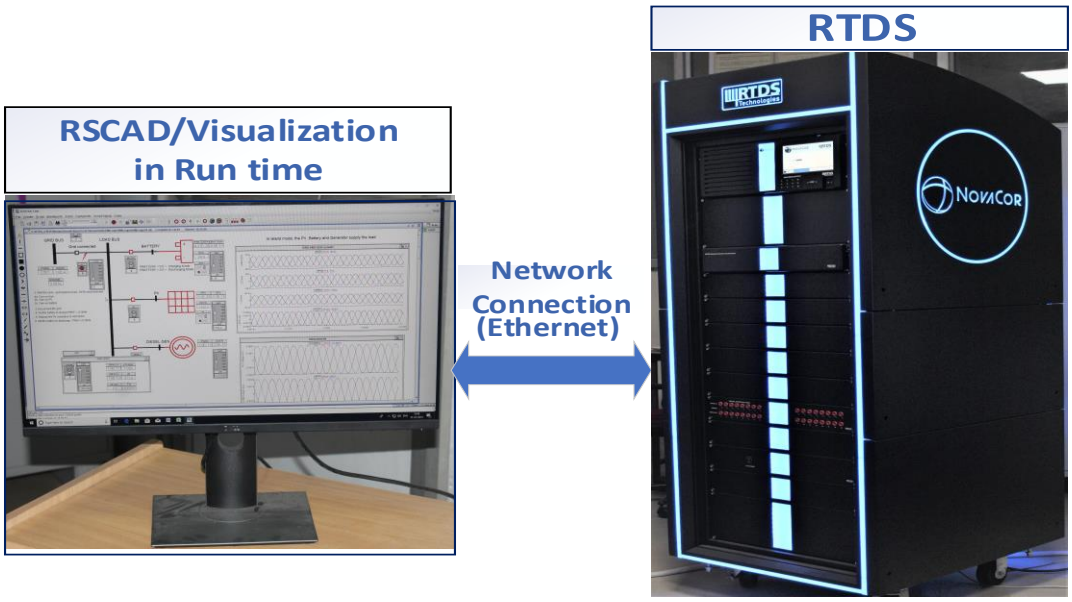

Figure 6.15: Schematic of RTDS (both software and hardware)

6.7.3.2 Real-time implementation under FTSC

In order to validate the droop control action in real-time, the instantaneous point at time period (14:00 to 14:15 h) and set point parameters as depicted in Table 6.3 have been used. The load demand is 91% of peak demand at this point and forecasted solar irradiation is 81% of the peak. During this time span, the lowest voltage profile at node 890 becomes vulnerable to any further reduction in kW power. The FTSC under cloud transient has been applied and illustrated without and with EV load penetrations as given in the following.

- *Case I. Cloud Transient Impact in the absence of EV Loads*

The sudden fall in solar irradiation from 0.81 to 0.4 kW/m^2 has been considered to analyze the cloud movement impact. Accordingly, the active power from the PVs plant has been reduced. As a result, drop in voltage occurs due to sudden fall in PV power output. This resulted in lower voltage limit violation, as seen from Figure 6.16, with red color line. Under the circumstances, the droop controller is enabled in order to rescue from voltage droop below the prescribed lower limit (as set in droop controller). The enabled droop controller

injects the additional VAR support to compensate the voltage deviation. It can be clearly seen from Figure 6.16 that droop control action is able to control the voltage profile locally. The node 890 is most vulnerable node for voltage deviation. Hence, the PV2 inverter reactive power dispatch is critical for droop operation. The reactive power (Q) support by PV2 inverter with and without droop controller has been shown in Figure 6.17. The reactive power dispatch with droop controller indicates the reactive power that is additive to centralized PV2 reactive power dispatch.

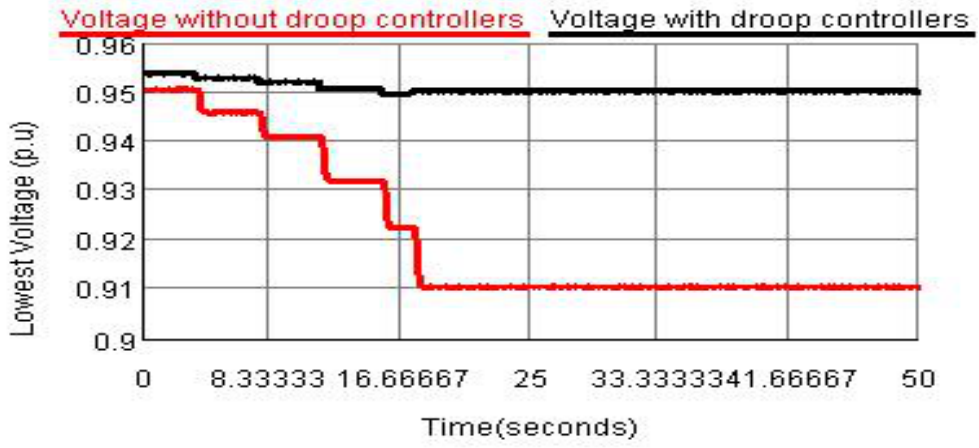

Figure 6.16 Lowest voltage profile without and with droop controllers

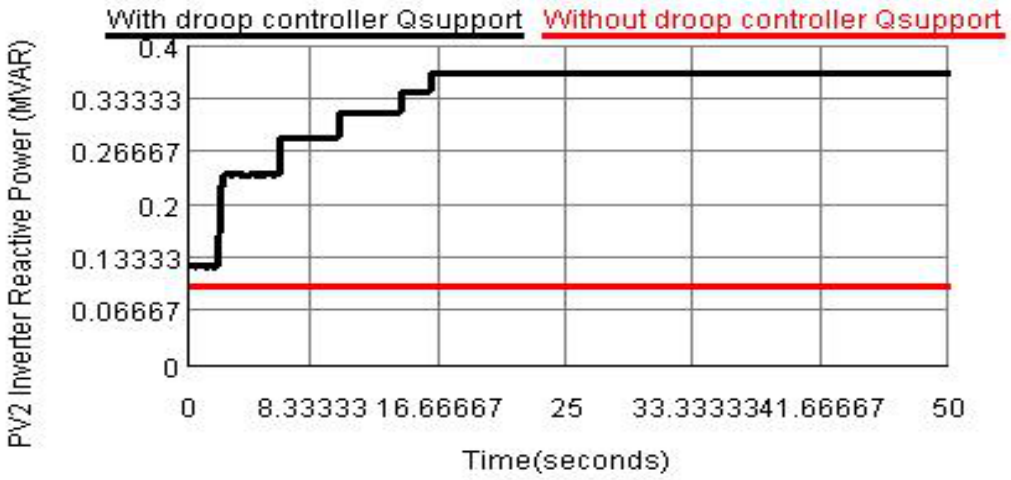

Figure 6.17 PV inverter reactive power compensation without and with droop controls

- *Case II. Cloud Transient Impact in Presence of EV Loads*

In this case, the sudden drop in solar irradiation from 0.81 to 0.3 kW/m^2 is observed due to the cloud movement. Figure 6.18 shows the lowest voltage profile. In both scenarios, when only PV inverters and combined PV and EV inverters are providing the droop-based VAR support. Figure 6.18 clearly shows that up to 0.4 kW/m^2 reduction in solar irradiation, VAR compensation from PV inverters, is alone proficient to maintain the lower voltage limit. However, after further reduction, PV inverters alone are not capable of maintaining the lower voltage limit. This is due to PV2 inverter having already reached its maximum allowable reactive power capacity. In such conditions, EV inverters from the charging station equipped with droop control feed the additional VAR support. Figure 6.18 clearly shows that after injecting the VAR from EV inverters, the lower voltage violation has been mitigated. Figure 6.19 shows the compensated VAR support from PV2 and EV inverter at node 890.

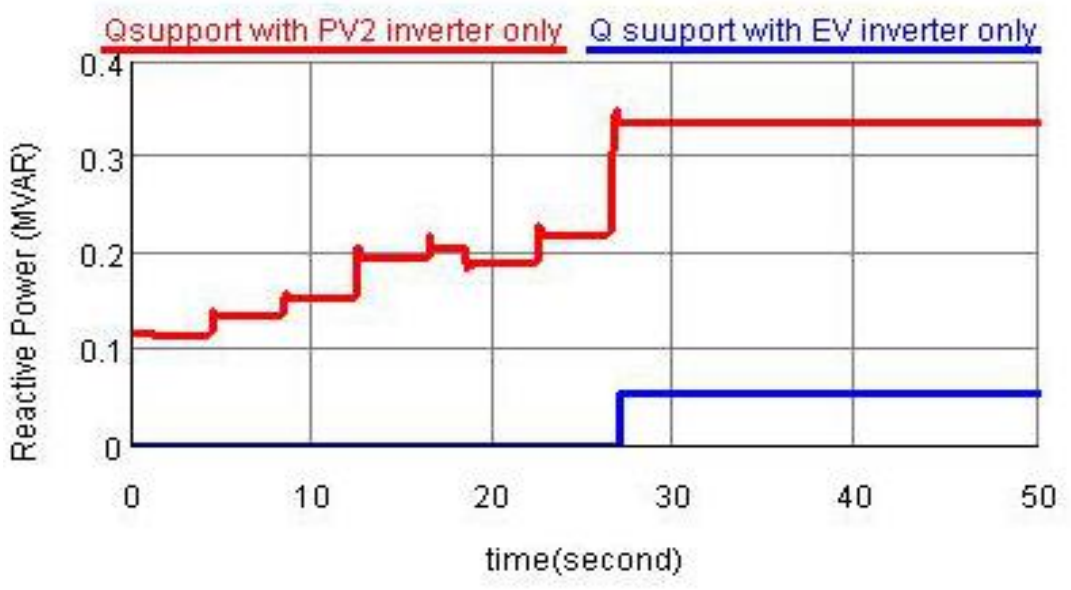

Figure 6.18. Lowest voltage profile with PV and EV inverters VAR support

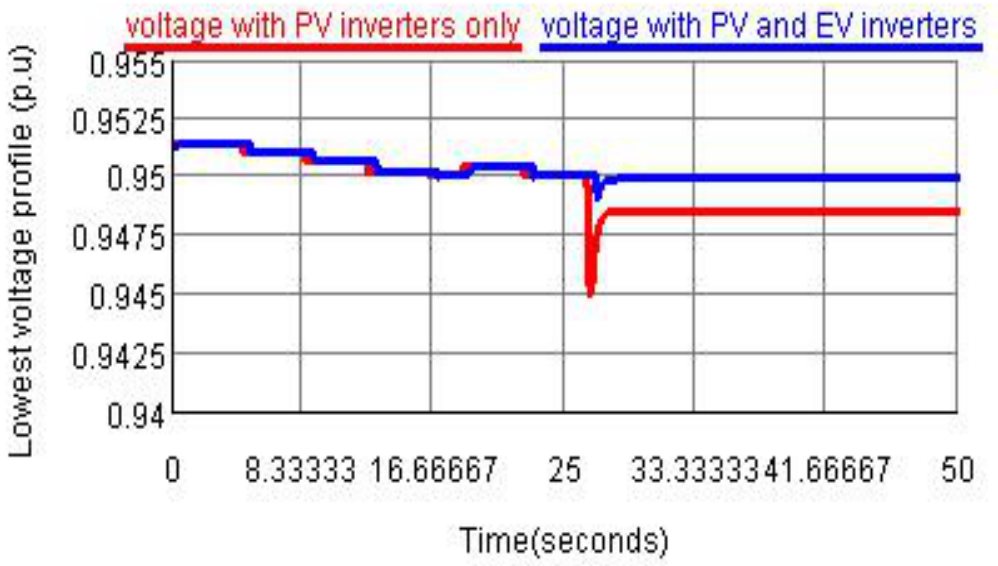

Figure 6.19. Compensated VAR support from PV2 and EV inverter at node 890

6.8 Conclusion

An investigation on CVR energy savings and impact of EV penetration in ADN has been carried out. A time horizon-based model predictive control method has been employed to handle the uncertainties in the system. The impact of different charging levels has been included in VVO formulation. Apart from PV inverters, the provision of reactive power support through EV charging station has been examined during centralized as well as local control. Most of the current EVs exhibit the constant power load characteristics; hence, CVR saving would reduce as EV penetration increases. Besides, the dynamic voltage control using VVD controller has been implemented on RTDS platform. The major findings of the present investigations are as follows.

- Significant reduction in energy demand, system losses, and saving in operating costs have been achieved with MP-VVO based CVR.

- The developed control method is capable of handling uncertainty and intermittency, such as cloud transient, without violating the feeder voltage profile.
- Reactive power compensation through EV charging stations may be a potential candidate for VAR support in the future.
- The simulation results show that EV charging load characteristics also influence the energy savings achieved by CVR.

The implementation of a real-time droop controller validates the proposed dynamic voltage control scheme. Thus, it can be concluded that enabling the CVR through proposed MP-VVO method yields better performance in terms of energy savings, cost savings, and voltage profile improvement even in the presence of EV charging loads.